BMC Medical Imaging

RESEARCH

Open Access

In vitro detection of cancer cells using a novel fluorescent choline derivative

Anna E. Caprifico[1*], Luca Vaghi[2], Peter Spearman[3], Gianpiero Calabrese[3] and Antonio Papagni[2]

Abstract

Introduction The treatment of preinvasive lesions is more effective than treating invasive disease, hence detecting cancer at its early stages is crucial. However, currently, available screening methods show various limitations in terms of sensitivity, specificity, and practicality, thus novel markers complementing traditional cyto/histopathological assessments are needed. Alteration in choline metabolism is a hallmark of many malignancies, including cervical and breast cancers. Choline radiotracers are widely used for imaging purposes, even though many risks are associated with their radioactivity. Therefore, this work aimed to synthesise and characterise a non-radioactive choline tracer based on a fluorinated acridine scaffold (CFA) for the in vitro detection of cervical and breast cancer cells by fluorescence imaging.

Methods CFA was fully characterised and tested for its cytotoxicity on breast (MCF-7), cervical (HeLa), glioblastoma (U-87 MG) and hepatoblastoma (HepG2) cancer cell lines and in normal cell lines (epithelial, HEK-293 and human dermal fibroblasts, HDFs). The cellular uptake of CFA was investigated by a confocal microscope and its accumulation was quantified over time. The specificity of CFA over mesenchymal origin cells (HDFs), as a model of cancer-associated fibroblasts was investigated by fluorescence microscopy.

Results CFA was toxic at much higher concentrations (HeLa $IC_{50} = 200 \pm 18$ μM and MCF-7 $IC_{50} = 105 \pm 3$ μM) than needed for its detection in cancer cells (5 μM). CFA was not toxic in the other cell lines tested. The intensity of CFA in breast and cervical cancer cells was not significantly different at any time point, yet it was greater than HepG2 and U-87 MG ($p \leq 0.01$ and $p \leq 0.0001$, respectively) after 24 h incubation. A very weak signal intensity was recorded in HEK-293 and HDFs ($p \leq 0.001$ and $p \leq 0.0001$, respectively). A selective ability of CFA to accumulate in HeLa and MCF-7 was recorded upon co-culture with fibroblasts.

Conclusions The results showed that CFA preferentially accumulated in cancer cells rather than in normal cells. These findings suggest that CFA may be a potential diagnostic probe for discriminating healthy tissues from malignant tissues due to its specific and highly sensitive features; CFA may also represent a useful tool for *in vitro/ex vivo* investigations of choline metabolism in patients with cervical and breast cancers.

Keywords Choline, Fluorescent dye, Biomarker, Tracer, Cellular uptake, Cervical cancer, Breast cancer

*Correspondence:
Anna E. Caprifico
anna.caprifico@dmu.ac.uk
[1]School of Allied Health Sciences, Faculty of Health & Life Sciences, De Montfort University, The Gateway, Leicester LE1 9BH, UK
[2]Department of Material Sciences, University of Milano-Bicocca, Via Roberto Cozzi 55, Milan 20126, Italy
[3]School of Life Sciences, Pharmacy and Chemistry, Kingston University London, Penrhyn Road, Kingston Upon Thames, London KT1 2EE, UK

Introduction

Cervical and breast cancers represent the leading causes of cancer-related deaths in women worldwide even though they are easily preventable [1]; cervical and breast screening programs are offered to all women aged between 25 and 50 years, respectively [2]. Cervical cancer starts from the uterine cervix and is mostly caused by an enduring infection with human papillomavirus (HPV), which activates oncogenes leading to the development of preinvasive cervical intraepithelial neoplasia and invasive cervical carcinoma [3]. The detection of infection is considered a useful marker for its diagnosis [3, 4]. Breast cancer may be caused by multiple factors: the presence of steroid hormone receptors (HRs) and the presence of tumour-infiltrating lymphocytes (TILs) are the main prognostic factors [5]. Breast cancer is currently detected in clinics using several techniques, such as gene expression assays, the Breast Cancer Index (BCI) [6], and the Genomic Grade Index (GGI) [7]. In addition, mammography using low-dose X-rays is employed as a preventative measure; indeed, this technique can provide high-quality images, detecting breast cancer before it is palpable and has spread to the axillary nodes [8]. Ultrasound, X-rays and magnetic resonance are also some of the techniques used to detect other types of tumours such as those affecting the liver and brain [9, 10].

Early detection of cancer is crucial because the treatment of preinvasive lesions is significantly more effective than treating the invasive disease. However, there is no screening method available that is highly sensitive, specific, affordable and practical. Consequently, there is a pressing need to identify markers that can complement traditional cyto/histopathological assessments and detect abnormal cells within a healthy tissue [11]. The latter is made of multiple cell types including adipocytes, and immune and mesenchymal cells, participating in the formation of the tumour microenvironment (TME), essential for tumour initiation and development. Cancer-associated fibroblasts (CAFs), also called myofibroblasts, are a heterogeneous population of mesenchymal cells representing the most abundant cells in the TME. CAFs release various molecules such as metalloproteinases, growth factors, cytokines and extracellular matrix (ECM) promoting key events of cancer progression including proliferation, angiogenesis, migration, invasion, epithelial-mesenchymal transition (EMT) and resistance to therapy [12, 13].

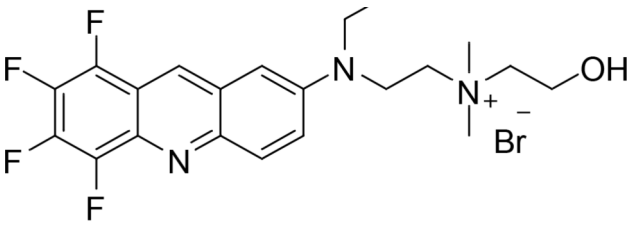

1

Fig. 1 Chemical structure of choline-based fluorinated acridine (CFA) **1**

Abnormal and uncontrolled cell proliferation are key features of cancer, mainly because of genetic and epigenetic changes regulating cell growth, differentiation and cell death [11]. A commonly used biomarker for cancer detection is choline, due to its high metabolism in cancer cells. Choline is an essential nutrient involved in several cellular functions, lipid metabolism, and cellular membranes' composition [14]. Morozov et al. [15] provided a review of the role of choline in cell life and its potential as a biomarker of different pathologies. Indeed, in the last 20 years, much research has focused on targeting cancer cells through choline phospholipid metabolism [16–18]. However, the main drawback of choline metabolism research is the predominant use of radiotracers (^{11}C-choline or ^{18}F-fluoromethylcholine). Radiotracers are highly specific and produce real-time and defined images; however, they have a short half-life and need to be stored and handled safely [19]. To overcome the problems associated with radioactivity, our group previously generated a non-radioactive choline tracer, using self-fluorescence for detecting living breast cancer cells, and demonstrated preferential accumulation in breast cancer cells compared to normal cells [20].

In the present study, we synthesised a novel probe in which choline is linked to a fluorinated acridine (choline fluorinated acridine – CFA (**1**), Fig. 1), acting both as a fluorescent dye and a DNA intercalator. This enables its intracellular visualisation by fluorescence imaging (FI) while also being a powerful and selective cytotoxic agent [21–23]. We selected a fluorinated acridine scaffold to increase bioavailability since fluorination enhances the hydrophobic interactions with choline transporters [24]. Moreover, we sought to exploit the peculiar optical properties of fluorinated acridine systems [23, 25]. The effects of the choline derivative tracer on both cervical and breast tumour cells were tested in terms of cellular uptake and cytotoxicity. Other cancer cell lines (glioblastoma and hepatocellular carcinoma) were also tested for comparison. Finally, the specificity toward cancer cells was investigated against two normal cell lines of both epithelial and mesenchymal origin to simulate the CAFs of the TME.

CFA is a water-soluble molecule, and the results showed that it was cytotoxic in a dose-dependent manner. Its emission lies in the visible region; hence, it was easily visualised in tumour cells by FI. These results suggested the potential role of CFA (**1**) as an *in vitro/ex vivo* tracer for cervical and breast cancer cells.

Materials and methods

Materials

All reagents and solvents needed for the synthesis of CFA (**1**) were purchased from commercial sources (Fluorochem Co.; Tokyo Chemical Industry Co. BLD Co. and Aldrich Chemical Co.) and used as received. Chromatographic purifications were performed using Merck 9385 silica gel (pore size 60 Å; 230–400 mesh). Dulbecco's minimum essential medium (DMEM), penicillin/streptomycin, phosphate-buffered saline (PBS), 3-(4,5-dimethylthiazol-2-yl)-2,5-diphenyltetrazolium bromide (MTT), dimethyl sulfoxide (DMSO), and fetal bovine serum (FBS) were purchased from Merck Millipore (UK).

Chemical characterisation

Melting points were measured with a Stanford Research Systems Optimelt apparatus. Infra-red (IR) spectra were recorded with a Perkin Elmer Spectrum 100 FT-IR spectrometer equipped with a universal ATR sampling accessory. ^{1}H, ^{13}C and ^{19}F NMR were recorded with a Bruker AVANCE III HD 400 MHz spectrometer (^{1}H: 400 MHz, ^{13}C: 101 MHz, ^{19}F: 376 MHz). Chemical shifts (δ) are expressed in parts per million (ppm), and coupling constants are given in Hz. Splitting patterns are indicated as follows: s=singlet, d=doublet, t=triplet, q=quartet, m=multiplet, br=broad. Elemental analyses were obtained with an Elementar Vario MICRO cube instrument.

Synthesis

2-[Ethyl(5,6,7,8-tetrafluoroacridin-2-yl)amino]ethanol (**3**). A solution of pentafluorobenzaldehyde (**2**) (0.7 g, 3.6 mmol), DABCO (1.6 g, 14.4 mmol) and 2-[(4-aminophenyl)(ethyl)amino]ethanol sulfate (2.0 g, 7.2 mmol) in decahydronaphthalene (40 mL) was heated at 175 °C for 72 h under a nitrogen atmosphere. After cooling to room temperature (rt), the crude mixture was purified by column chromatography (SiO_2, CH_2Cl_2/EtOH 98:2) to afford **3** (650 mg, 53%). Orange solid; mp 184 °C; ^{1}H NMR (400 MHz, $CDCl_3$) δ 8.59 (s, 1H), 8.14 (d, *J*=9.7 Hz, 1H), 7.64 (dd, *J*=9.7, 2.9 Hz, 1H), 6.90 (d, *J*=2.8 Hz, 1H), 3.94 (t, *J*=5.8 Hz, 2 H), 3.67 (t, *J*=5.8 Hz, 2 H), 3.61 (q, *J*=7.1 Hz, 2 H), 1.84 (br, 1H), 1.29 (t, *J*=7.1 Hz, 3 H); ^{13}C NMR (101 MHz, $CDCl_3$) δ 146.4 (s), 144.9 (s), 143.6–142.9 (m), 141.7–140.3 (m), 139.1–137.7 (m), 130.5 (s), 128.5 (s), 124.7 (s), 124.0 (s), 122.9–122.3 (m), 115.4 (d, *J*=15.9 Hz), 113.3 (s), 101.8 (s), 60.3 (s), 52.4 (s), 45.7 (s), 12.1 (s); ^{19}F NMR (376 MHz, $CDCl_3$) δ -152.17 (t, *J*=16.4 Hz), -153.00 (t, *J*=15.8 Hz), -157.28 (t, *J*=16.2 Hz), -159.35 (t, *J*=17.0 Hz); IR (ATR) 3315, 2979, 2955, 2893, 1679, 1615, 1593, 1501, 1491, 1463, 1426, 1367, 1339, 1286, 1250, 1238, 1163, 1127, 1082, 1058, 1025, 998, 950, 901, 822, 806, 774, 665, 603, 575 cm^{-1}; Anal. Calcd. For $C_{17}H_{14}F_4N_2O$: C, 60.36; H, 4.17; N, 8.28. Found: C, 60.58; H, 4.12; N, 8.19. (Additional file 1)

***N*-(2-bromoethyl)-*N*-ethyl-5,6,7,8-tetrafluoroacridin-2-amine** (**4**). 2-[ethyl(5,6,7,8-tetrafluoroacridin-2-yl)amino]ethanol (**3**) (650 mg, 1.92 mmol) and CBr_4 (776 mg, 2.34 mmol) were dissolved in dry CH_2Cl_2 (33 mL) under a nitrogen atmosphere. The solution was cooled to 0 °C and PPh_3 (613 mg, 2.34 mmol) was added. After stirring for 10 min, the reaction mixture was allowed to warm to rt and left under stirring overnight. The solvent was then removed under reduced pressure, and the residue was purified by column chromatography (SiO_2, first CH_2Cl_2/heptane 1:1, then CH_2Cl_2) to afford **4** (473 mg, 61%). Yellow solid; mp 172 °C; ^{1}H NMR (400 MHz, $CDCl_3$) δ 8.51 (s, 1H), 8.10 (d, *J*=9.7 Hz, 1H), 7.52 (dd, *J*=9.7, 2.9 Hz, 1H), 6.80 (d, *J*=2.8 Hz, 1H), 3.85 (t, *J*=7.8 Hz, 2H), 3.71–3.45 (m, 4H), 1.31 (t, *J*=7.1 Hz, 3H); ^{13}C NMR (101 MHz, $CDCl_3$) δ 145.1 (s), 144.7 (s), 143.3–140.4 (m), 141.5–138.6 (m), 138.5–137.6 (m), 135.5 (t, *J*=16.3 Hz), 132.4 (d, *J*=10.7 Hz), 130.8 (s), 128.2 (s), 124.8 (d, *J*=6.1 Hz), 123.0 (s), 115.2 (d, *J*=14.7 Hz), 101.6 (s), 52.3 (s), 45.6 (s), 27.9 (s), 12.7 (s); ^{19}F NMR (376 MHz, $CDCl_3$) δ -151.99 (t, *J*=16.7 Hz), -152.89 (t, *J*=16.0 Hz), -157.05 (t, *J*=16.5 Hz), -159.16 (t, *J*=17.2 Hz).; IR (ATR) 3083, 3060, 3038, 2986, 2927, 2870, 1682, 1618, 1593, 1495, 1459, 1424, 1358, 1342, 1262, 1218, 1202, 1150, 1103, 1072, 1026, 994, 941, 904, 816, 658, 643, 541 cm^{-1}; Anal. Calcd. For $C_{17}H_{13}BrF_4N_2$: C, 50.89; H, 3.27; N, 6.98. Found: C, 50.82; H, 3.30; N, 7.01. (Additional file 2)

2-[Ethyl(5,6,7,8-tetrafluoroacridin-2-yl)amino]-*N*-(2-hydroxyethyl)-*N*,*N*-dimethylethanaminium bromide (**1**). Dimethylethanolamine (200 mg, 2.24 mmol) was slowly added to a 0 °C solution of **4** (450 mg, 1.12 mmol) in dry THF (5 mL) under a nitrogen atmosphere. The mixture was allowed to reach rt and then stirred at 50 °C overnight. The solid formed was filtered and washed extensively with cold diethyl ether to afford **1** (200 mg, 41%). Brown solid; ^{1}H NMR (400 MHz, D_2O) δ 7.64 (s, 1H), 7.40–7.23 (m, 2 H), 6.34 (d, *J*=1.4 Hz, 1H), 4.10 (s, 2H), 3.88–3.81 (m, 2 H), 3.66–3.54 (m, 4H), 3.40 (dd, *J*=13.8, 6.7 Hz, 2H), 3.29 (s, 6 H), 1.18 (t, *J*=7.0 Hz, 3 H); ^{13}C NMR (101 MHz, D_2O) δ 144.7 (s), 141.4 (s), 141.0–138.1 (m), 139.9–137.1 (m), 139.4–136.3 (m), 136.2–133.2 (m), 128.9 (d, *J*=9.0 Hz), 127.2 (s), 126.2 (s), 124.0 (s), 123.1 (s), 113.3–112.3 (m), 100.6 (s), 65.5 (s), 58.7 (s), 55.4 (s), 55.1 (s), 51.9 (s), 42.6 (s), 11.3 (s); ^{19}F NMR (376 MHz, D_2O) δ -151.94 (s), -154.37 (s), -156.97 (s), -159.66 (s); IR (ATR) 3302, 3033, 2977, 1682, 1618, 1591, 1503, 1488, 1427, 1367, 1342, 1250, 1184, 1158, 1077, 1026, 997, 961, 945, 917, 825, 817, 776, 656, 603, 562 cm^{-1}; Anal. Calcd. For $C_{21}H_{24}BrF_4N_3O$: C, 51.44; H, 4.93; N, 8.57. Found: C, 51.33; H, 4.98; N, 8.64. (Additional file 3)

Characterisation of spectral properties

The absorption spectra of CFA (**1**) in PBS (100 µM) were recorded using an Agilent Cary Ultra visible (UV–Vis) spectrophotometer. Photoluminescence measurements were carried out on a Cary Eclipse Fluorescence Spectrophotometer.

Cell culture

HeLa (human cervical cancer), MCF-7 (adenocarcinoma, human breast cancer), U-87 MG (glioma, human), HepG2 (hepatoblastoma, human), HEK-293 (human embryonic kidney) and HDFs (human dermal fibroblasts) were obtained from De Montfort University. All cell lines were maintained in DMEM supplemented with 10% FBS, 100 µg/mL penicillin/streptomycin and grown at 37 °C in a 5% CO_2 humidified atmosphere.

In vitro cell toxicity study

Cells were seeded in a 96-wells plate at 0.05×10^6 cells/mL in a supplemented medium (100 µL) and grown overnight. The cells were then incubated with increasing concentrations of CFA (**1**) (5, 12.5, 25, 50, 100 and 200 µM) for 72 h. The cell viability was then assessed using the MTT assay: water-soluble MTT is converted into water-insoluble purple formazan in metabolically active cells by the action of mitochondrial reductase, and the amount of formazan produced is directly proportional to the number of living cells [26]. Briefly, MTT (20 µL, final concentration of 0.5 mg/mL) was added to each well and incubated for 4 h at 37 °C in the dark. After discarding the medium, the cells were carefully washed with PBS to remove any residual fluorescent compound, and the formazan products were dissolved in DMSO (100 µL). The plate was then shaken for 15 min at rt in the dark, after which the absorbance was measured at 550 nm with a reference at 690 nm [26]. The experiment was run in triplicate. The cell viability was expressed as a percentage (%) and calculated by dividing the absorbance of the cells treated with CFA (**1**) by the absorbance of the control (cells treated with medium only). IC_{50} values were extrapolated from the graph generated by plotting cell viability data against concentrations of CFA [27].

Cellular uptake of CFA by cells over time

Cells were plated onto 24 wells optically clear tissue culture plate at 0.1×10^6 cells/well and grown overnight. The cells were then incubated with 5 µM of CFA (**1**) for 0, 2, 4, 6, 16 and 24 h. The experiment was run in triplicate. At each time point, the cells were washed with PBS, fixed with paraformaldehyde (4%) for 20 min and rehydrated in PBS for 1 h at rt. The specimens were stored at 4 °C until examination, performed using a confocal microscope (Zeiss Axiovert 200 M, Oberkochen, Germany) equipped with a 20× objective and a laser scanning microscope (LSM) 5 image browser (Carl Zeiss, Oberkochen, Germany). To allow a direct comparison of the absolute intensity of different time points, imaging setup was kept constant throughout all the experiments: a 488 nm laser with 0.2% power and 28 µm pinhole was employed; with the help of the "range indicator" feature of ZEN, the threshold of detection was adjusted so to ensure a linear range of detection [28]: the sensitivity of the detectors (Master Gain) was set at 700 V and the noise was minimised by setting the Digital Offset at 0 and the Digital Gain at 1.

Quantification of microscope fluorescence intensity (MFI)

ImageJ software (NIH, USA) was used to quantify the signal intensity corresponding to CFA as described by Shihan et al. [28]. Briefly, an external drawing pen was used to circle the desired area (Region of Interest, ROI); the software automatically generated a pixel value corresponding to the microscope fluorescence intensity (MFI). The MFI of samples was normalised by subtracting the background MFI (non-fluorescent area of the negative control) from the MFI of the ROI using Excel.

Detection limit

The detection limit was obtained from the fluorescence titration data based on a previous report [29]. Briefly, each cell line was plated in a 24-well plate at increasing cell density (1300, 2600, 7800, 14000, 21000 and 56000 cells/cm^2) and grown overnight. Cells were then incubated at 37 °C in a 5% CO_2 humidified atmosphere with 5 µM of CFA (**1**) for 24 h, to allow maximum cellular uptake. The experiment was run in triplicate. The fluorescence intensity of the supernatant was then measured using the Cary Eclipse Fluorescence Spectrophotometer, at 566 nm. The amount of CFA accumulated by the cells was calculated by subtracting the values of fluorescence intensity of the supernatant from the medium containing the initial concentration of CFA. The fluorescence spectrum of the medium only (blank) was measured five times and the standard deviation was calculated. To gain the slope, the fluorescent intensity data at 566 nm was plotted as cell density (cells/cm^2). The detection limit of CFA for each cell line was obtained using Eq. (1):

$$Detection\ limit = \frac{3\sigma}{K} \tag{1}$$

Where "σ" is the standard deviation of blank measurement, and "K" is the slope between the fluorescence intensity *versus* cell densities (cells/cm^2).

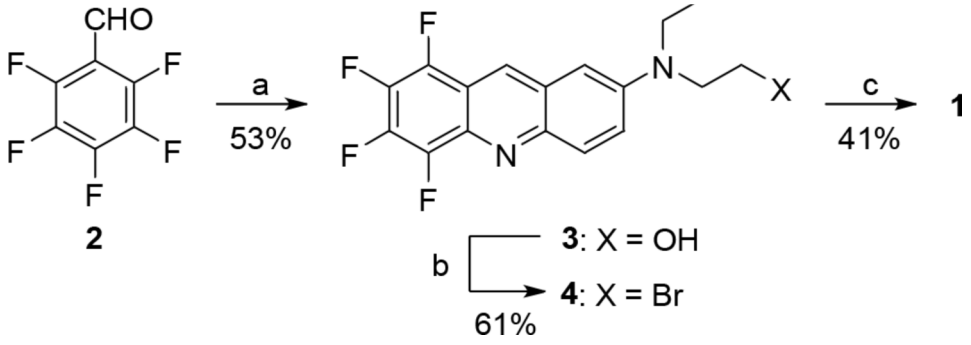

Scheme 1 Synthesis of **1**. Reagents and conditions: [a] 2-((4-aminophenyl)(ethyl)amino)ethanol sulfate (2 equiv), DABCO (4 equiv), decahydronaphthalene, 175 °C, 72 h, N_2; [b] CBr_4 (1.2 equiv), PPh_3 (1.2 equiv), CH_2Cl_2, 0 °C to rt, 16 h, N_2; [c] 2-(dimethylamino)ethanol (1.5 equiv), THF, 50 °C, 72 h, N_2

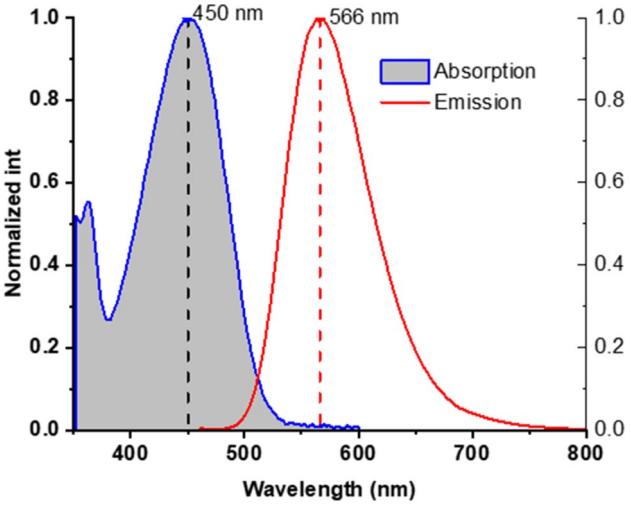

Fig. 2 Normalised absorption and emission spectra of CFA (1) in PBS (100 µM)

CFA selectivity toward cancer cells in a co-culture with normal fibroblasts

To investigate the ability of CFA to selectively accumulate in breast and cervical cancer cells, normal HDFs were plated in a 24-wells plate at 0.1×10^6 cells/well and grown overnight; HeLa and MCF-7 cells were then plated at a density corresponding to their respective limit of detection and allow to adhere overnight. The co-culture was then treated with 5 µM of CFA for 24 h, to achieve the maximum cellular uptake. Images were taken using a Leica DM750 Fluorescence Microscope, equipped with a 10× objective. The following settings were used: transmitted light channel at 33%, blue channel at 41% and green channel at 43%. Fibroblasts only were taken as negative control and employed to adjust the settings.

Statistical analysis

The data are expressed as the mean ± standard deviation (SD). Statistical analyses were performed using one-way analysis of variance (ANOVA) with significance set at $p \leq 0.05$. A post-hoc test (Tukey multiple comparison test) was performed to determine differences between groups. All the statistical analyses were carried out using GraphPad Prism 9.3.1 (GraphPad Software, Inc.).

Results

Synthesis and characterisation of CFA (1)

CFA (**1**) was synthesised starting from pentafluorobenzaldehyde (**2**) (Scheme 1). Tandem nucleophilic aromatic substitution/thermal promoted electrocyclization-aromatisation by treatment with in-situ prepared 2-[(4-aminophenyl)(ethyl)amino]ethanol in decahydronaphthalene at 175 °C afforded 2-[ethyl(5,6,7,8-tetrafluoroacridin-2-yl)amino]ethanol (**3**) [30, 31]. **3** was then converted into *N*-(2-bromoethyl)-*N*-ethyl-5,6,7,8-tetrafluoroacridin-2-amine (**4**) by reaction with CBr_4 and triphenylphosphine [32]. Finally, treatment of **4** with 2-(dimethylamino)ethanol allowed the formation of **1**.

Figure 2 shows the absorption–emission spectra of CFA (**1**), with a Stokes shift (116 nm (0.57 eV)) between the absorption and emission maxima (450 nm and 566 nm, respectively).

Dose-dependent cell toxicity of CFA toward cervical and breast cancer cells

The ability of CFA (**1**) to inhibit the cellular metabolic activity in a dose-dependent manner was determined using the MTT assay (Fig. 3). The viability was above 80% when a concentration of CFA up to 12.5 µM was used after an incubation time of 72 h, while a sharp decrease in cell viability was recorded at higher concentrations for the cell lines under investigation, except HepG2 whose viability remained above 90% when concentrations of CFA up to 200 µM were used. The IC_{50} values determined for HEK-293 and HDFs (Fig. 3A), U-87 MG and HepG2 (Fig. 3B) were above the tested range of concentrations. The IC_{50} values determined for HeLa and MCF-7 cells (Fig. 3C) were 200 ± 18 µM and 105 ± 3 µM, respectively, suggesting that MCF-7 cells were more susceptible to the cytotoxic action of CFA than HeLa cells.

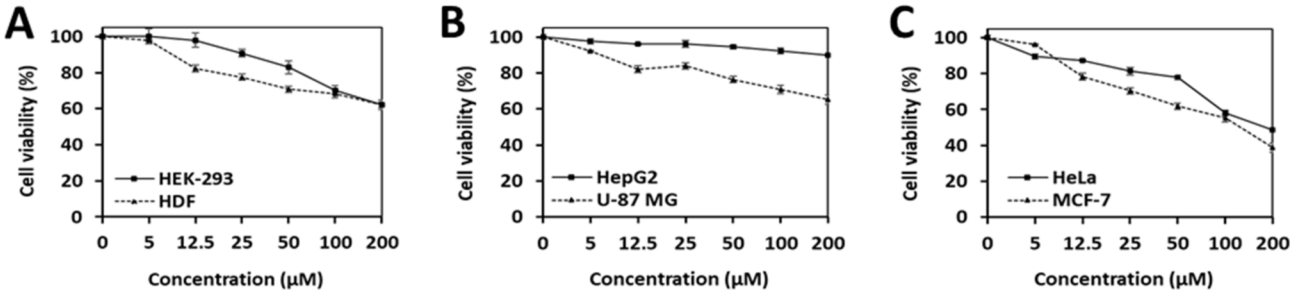

Fig. 3 Cell viability (%) of the tested cell lines. **A**) Normal cell lines: HEK-293 and HDF; **B**) Other types of cancer cell lines: HepG2 and U-87 MG; **C**) Cancer cell lines of interest: HeLa and MCF-7. Cells were incubated with increasing concentrations (5, 12.5, 25, 50, 100 and 200 μM) of CFA (**1**) for 72 h. Cell viability was determined using the MTT colourimetric assay. The data are presented as the mean of three independent experiments. The lines shown are error bars

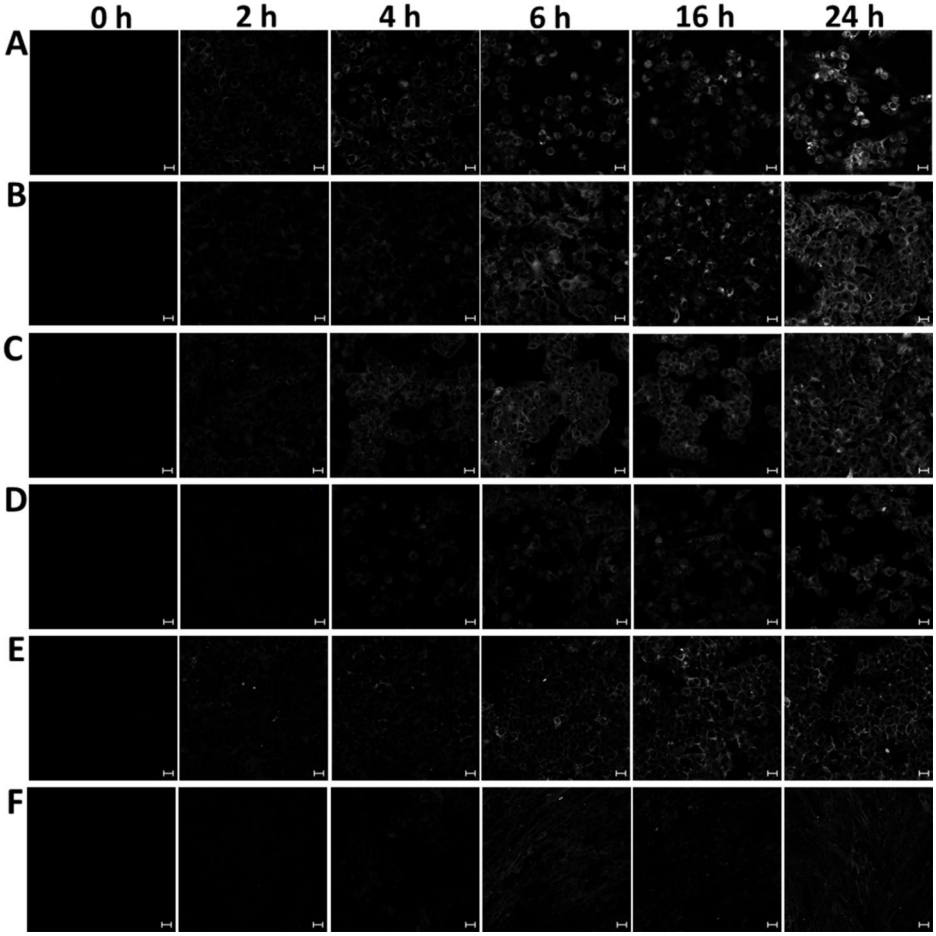

Fig. 4 Confocal images of cell lines treated with CFA (5 μM) at increasing incubation time. **A**) HeLa, **B**) MCF-7, **C**) HepG2, **D**) U-87 MG, **E**) HEK-293 and **F**) HDF cells. After each time point (0, 2, 4, 6, 16 and 24 h), cells were washed with PBS, and fixed with paraformaldehyde before being observed under a confocal microscope using a 20x objective. To allow a direct comparison of the absolute intensity of different time points, imaging setups were kept constant throughout all the experiments. Images are representative of three fields of vision taken from the same sample. Scale bar: 20 μm

Time-dependent cellular uptake of CFA

The cellular uptake of CFA (**1**) by each cell line was tested over time (from 0 to 24 h): at each time point, cells were washed and fixed before being observed using a confocal microscope. The excitation of the fluorescent dye was carried out at a wavelength within the absorption band of the fluorinated acridine moiety (488 nm laser), keeping the confocal microscope settings constant throughout the observations. The cellular uptake of CFA was quantified and expressed as MFI values. Before 6 h incubation, a low signal of CFA (**1**) was observed in HeLa cells (Fig. 4A), becoming more evident after 6 h ($p \leq 0.0001$,

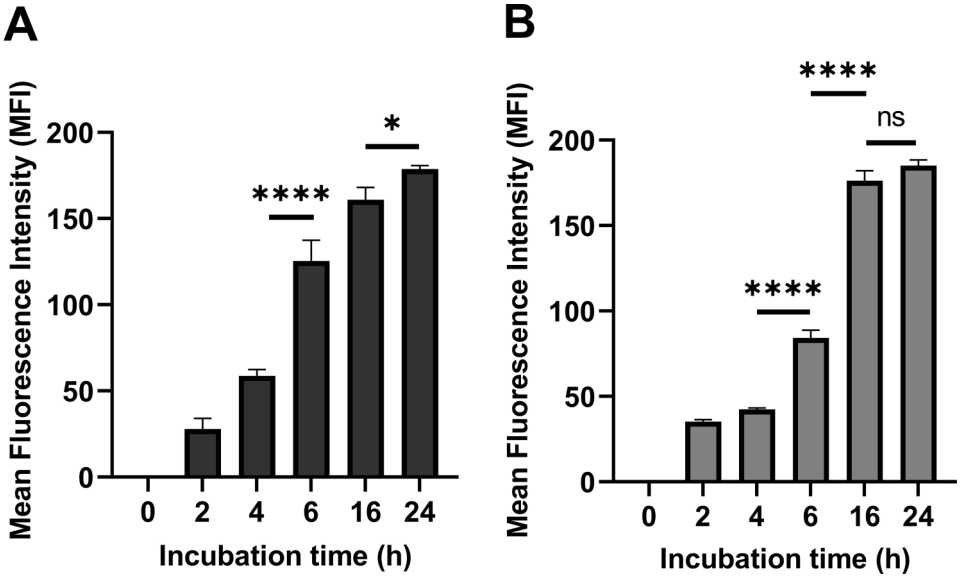

Fig. 5 Mean fluorescence intensity (MFI) at increasing incubation time (h) upon incubation with CFA (5 µM). **A**) MFI of CFA in HeLa cells; **B**) MFI of CFA in MCF-7 cells. The MFI of samples was normalised by subtracting the background MFI (non-fluorescent area of the negative control) from the MFI of the ROI using Excel. The data are presented as the mean of three independent experiments. The lines shown are error bars. Asterisks indicate statistical significance: *$p \leq 0.05$ and ****$p \leq 0.0001$; ns, non-significant

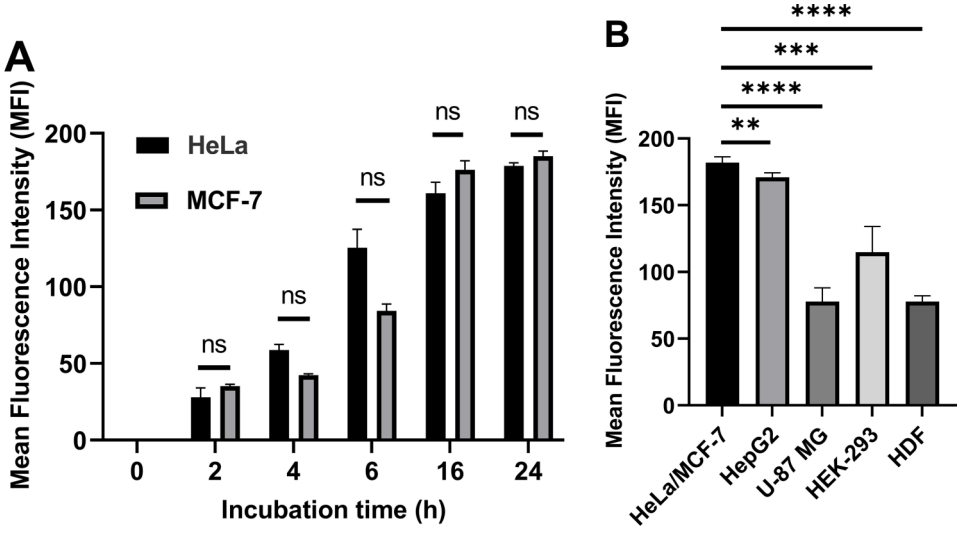

Fig. 6 Mean fluorescence intensity (MFI). **A**) MFI in HeLa vs. MCF-7 cells treated with 5 µM of CFA over 0, 2, 4, 6, 16 and 24 h. **B**) MFI in HeLa or MCF-7 versus other types of cancer cell lines (HepG2 and U-87 MG) and normal cell lines (HEK-293 and HDF) after 24 h incubation with 5 µM of CFA. MFI can be translated to the amount of CFA taken up by cells: the cellular uptake of CFA was time-dependent and significantly lower in other types of tumour cells (HepG2 and U-87 MG) and normal cells. The MFI of samples was normalised by subtracting the background MFI (non-fluorescent area of the negative control) from the MFI of the ROI using Excel. The data are presented as the mean of three independent experiments. The lines shown are error bars. Asterisks indicate statistical significance: **$p \leq 0.01$, ***$p \leq 0.001$ and ****$p \leq 0.0001$; ns, non-significant

Fig. 5A), increasing up to 24 h incubation ($p \leq 0.05$). The cellular uptake of CFA in MCF-7 cells (Fig. 4B) followed a similar pattern of HeLa cells up to 6 h incubation ($p \leq 0.0001$, Fig. 5B), showing a sharp increase following 16 h incubation ($p \leq 0.0001$) with no significant difference following 24 h incubation. No significant difference in the MFI values was recorded at any time point in HeLa cells compared to MCF-7 cells (Fig. 6A). Figure 4C shows the cellular uptake of CFA in HepG2 cells at increasing time points. The MFI of CFA became evident after 2 h incubation, but it was slightly lower than HeLa and MCF-7 cells following 24 h incubation ($p \leq 0.01$, Fig. 6B). The cellular uptake of CFA was less evident in U-87 MG cells at any time point (Fig. 4D), even after 24 h incubation ($p \leq 0.0001$, Fig. 6B). In HEK-293, the MFI of CFA become evident after 2 h of incubation while HDFs show a very

Table 1 The detection limit (cells/cm^2) of the tested cell lines toward CFA (1)

Cell line	Detection limit (cells/cm^2)
HeLa	2000 ± 145
MCF-7	5000 ± 363
HepG2	4000 ± 767
U-87 MG	3000 ± 300
HEK-293	14000 ± 300
HDF	53000 ± 625

low cellular uptake at increasing time points (Fig. 4E and F, respectively). Indeed, significantly lower MFI values of CFA were recorded after 24 h incubation in both normal cell lines, HEK-293 ($p \leq 0.001$) and HDF ($p \leq 0.0001$) compared to HeLa and MCF-7 cells (Fig. 6B).

Selective CFA uptake by cancer cells at their respective detection limit

The detection limit of each cell line toward CFA (**1**) is shown in Table 1. There was a good linearity between fluorescent intensity data at 566 nm and cell density ranging from 1300 to 56000 cells/cm^2, indicating that the probe can detect low cell density of HeLa and MCF-7 cells (2000 ± 145 and 5000 ± 362 cells/cm^2, respectively). A similar detection limit was found for other cancer cell lines such as HepG2 and U-87 MG (4000 ± 767 and 3000 ± 300 cells/cm^2, respectively). A higher detection limit was found for the normal cell lines: HEK-293 cells showed a detection limit of 14000 ± 300 cells/cm^2; the detection limit was considerably higher for HDFs (53000 ± 625 cells/cm^2). The linear equations for each cell line are shown in Additional File 4.

The selective cellular uptake of CFA (**1**) of HeLa and MCF-7 cells was qualitatively assessed in a co-culture with normal HDFs, plating MCF-7 and HeLa at their detection limit on top of the monolayer of HDFs. Images were taken by fluorescence microscopy (Fig. 7): data were normalised by setting the power of the green channel in a range that minimised the fluorescence emitted by HDFs only (control). A strong fluorescence green signal corresponding to CFA (**1**) was observed in some points (indicated by red arrows) which presumably corresponded to HeLa and MCF-7 cells (A. II and B. II, respectively), suggesting that CFA (**1**) was able to detect a small number of cancer cells embedded in a bed of fibroblasts, simulating the CAFs population.

Discussion

This study aimed to investigate the ability of a novel choline derivative (CFA) to act as a fluorescent choline tracer for tumours characterised by an increased metabolism of choline, such as cervical and breast cancer. The tracer was successfully synthesised, and its optical properties were characterised; the relatively large Stokes shift between the absorption and emission maxima of CFA (116 nm) is evidence of the charge-transfer nature of the transition. Since the transitions responsible for the emission and absorption reside on the acridine moiety, the tertiary amine can participate in the acridine conjugated system in the excited state, consequently increasing the extent of conjugation and effectively lowering the emission transition energy. Such a large Stokes shift minimises interference between the excitation and the fluorescence emission, prevents self-quenching and is highly suited for bioimaging. Indeed, CFA (**1**) possesses efficient optical properties that allow its intracellular detection at very low concentrations (5 µM) and incubation times with no induction of cell toxicity. Since acridine derivatives

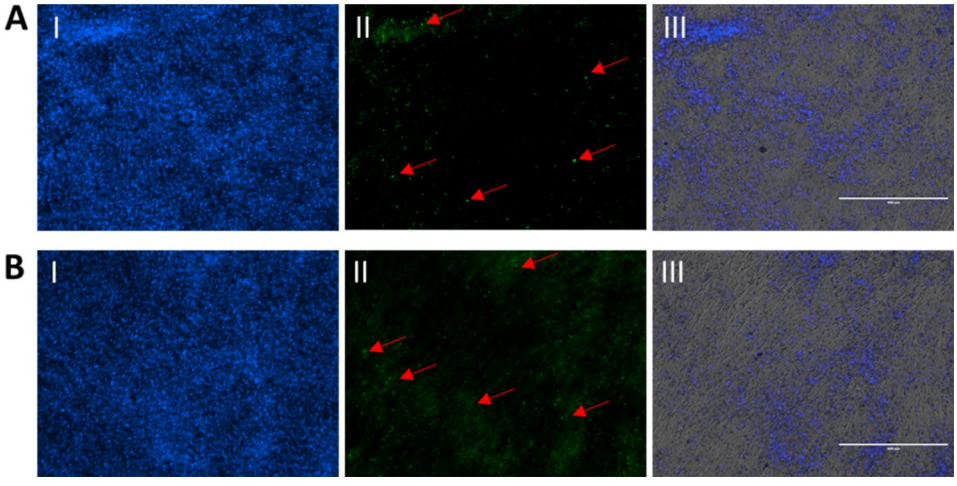

Fig. 7 Fluorescence microscopy images of HDFs along with cancerous cells. **A**) HeLa cells and **B**) MCF-7 cells, incubated with 5 µM CFA for 16 h. The surface of the cells was then washed twice to reduce nonspecific signals, and fluorescence images were taken using a 10× objective. (I) Nuclear staining using Hoechst 33342. (II) Green spots associated with cells that accumulated CFA, indicated by red arrows. (III) Transmitted light overlapped with Hoechst 33342 and CFA. Images are representative of three fields of vision taken from the same sample. Scale bar: 400 µm

generally have good inhibitory effects on topoisomerase I/II, cytotoxicity may be related to the inhibition of these enzymes. Several studies have explored acridine derivatives for their excellent anticancer activity [23, 33, 34]. As an acridine derivative, CFA (**1**) was screened for its cytotoxicity toward tumours and normal cells; the cytotoxic effects are expressed as the growth inhibitory concentration (IC_{50}), which represents the concentration needed to achieve 50% inhibition of cell growth after 72 h of incubation [35]. The IC_{50} values of CFA (**1**) indicated excellent growth inhibition of MCF-7 cells (100 µM), which was similar to that of other acridine derivatives compared to the reference drug doxorubicin (IC_{50}=65 µg/mL) [35]. The growth inhibitory effects of CFA (**1**) on HeLa cells were within the tested concentrations but lower than those on MCF-7 cells or other acridine derivatives and camptothecin [27, 36]. Other types of cancer cells (HepG2 and U-87 MG) and normal cell lines (HEK-293 and HDFs) showed a cell viability of over 60% upon treatment with CFA (**1**) at its highest concentration (200 µM). The selectivity in cell toxicity might be related to the higher uptake of CFA (**1**) after 24 h by MCF-7 and HeLa cells compared to the other cell lines tested. MCF-7 cells are a well-established cell line for studying altered phospholipid metabolism in breast cancer [20, 37, 38] since high choline levels were detected in these cancer cells [39]. However, previous studies also demonstrated high choline uptake by HeLa cells [40–42]. By comparison, this preliminary study suggested that choline uptake is greater in breast and cervical cancer compared to liver cancer and glioblastoma.

Regarding the detection limit of CFA (**1**), a very low cell density (ranging from 2000 to 5000 cells/cm^2) was needed to detect CFA (**1**) in the cancer cells, while a 2-fold and 10-fold higher cell density was needed to detect CFA (**1**) in normal epithelial cells (HEK-293) and fibroblasts (HDFs), respectively. HDFs were chosen in this study as a model of CAFs which interact with cancer cells in the tumour matrix. In the TME, normal fibroblasts act as tumour suppressor cells but, as the tumour advances, cancer cells turn fibroblasts into allies through the secretion of cytokines and growth factors, allowing fibroblasts to assist with proliferation, migration and invasion [43]. Wessels et al. [44] demonstrated that normal HDFs were able to turn themselves into CAFs upon treatment with a medium conditioned by a breast cancer cell line; cancer cells released fibroblast activation factors and cytokines such as IL-6 that activated HDFs. The population of CAFs originating from HDFs showed a shape, motility and gene expression similar to the CAF population originating from human primary mammary fibroblasts [44]. CAFs are characterised by an increased ability to proliferate and migrate compared to normal fibroblasts [13], hence, to employ CFA (**1**) in later stages of the disease, further studies are needed to establish a potential increased uptake of CFA (**1**) in activated HDFs. In this study, HDFs were not turned into CAFs, since the aim was to assess the selective accumulation of CFA (**1**) by cancer cells at an early stage of the disease, characterised by lower cancer cell density, while CAFs develop during cancer progression [13]. To this end, normal HDFs were successfully employed to show the selective ability of CFA (**1**) to preferentially accumulate in cancer cells rather than in normal ones. However, the TME is composed of a heterogeneous population of CAFs, made not only by fibroblasts but also by epithelial and endothelial cells converting themselves into CAFs via epithelial-mesenchymal transition (EMT) and endothelial–mesenchymal transition, respectively [45]. HEK-293 cells were employed as a model of normal epithelial cells and the cellular uptake of CFA (**1**) was compared to the tested cancer cell lines ($p \leq 0.001$). HEK-293 is an established normal cell line, characterised by high reliability and fast growth and is widely used in research to compare the effects of novel therapeutic agents with cancer cells [46]. Results showed a significantly lower cellular uptake of CFA (**1**) in HEK-293 cells compared to cancer cells. However, HEK-293 cells' high proliferation rate may lead to a higher cellular uptake of CFA (**1**) compared to normal epithelial cells of non-embryonic origin, suggesting that cellular uptake of CFA (**1**) in normal cells may be even lower. These results correlate well with our previous study [20] showing that choline and phosphatidylcholine fluorescent derivatives accumulated preferentially in malignant breast cells, in which choline uptake and metabolism were augmented [47, 48]. This feature is key for intravenous administration of the tracer since it allows specific accumulation in malignant cells while averting healthy cells. However, CFA (**1**) is suitable for in vitro or ex vivo studies or in vivo using specific instrumentation able to reach the area of interest since the UV−Vis light (100–800 nm) shows poor penetration depth (up to 2.5 mm) in biological tissues.

Conclusion

A novel fluorescent tracer based on choline was synthesised for the in vitro detection of cervical and breast cancers. The interaction of choline with fluorinated acridine (CFA) was tracked by self-fluorescence, and the compound was preferentially taken up by cancer cells compared to healthy cells ($p \leq 0.0001$). These results suggest that CFA (**1**) could be used as a potential biomarker in the context of early diagnosis of cancerogenic lesions. However, further ex-vivo studies that more closely simulate the cellular population of TME are needed. Due to its high sensitivity, specificity, and relatively ease of synthesis CFA has the potential to become a practical screening tool to complement existing diagnostic techniques in the context of cervical and breast cancer. To pursue this

goal, future studies will involve the application of CFA in tumoural in vivo tissues.

Abbreviations

CFA	Choline Fluorinated Acridine
HPV	Human Papilloma Virus
HR	Hormone Receptor
TIL	Tumour-Infiltrating Lymphocyte
BCI	Breast Cancer Index
GGI	Genomic Grade Index
DNA	Deoxyribonucleic Acid
TME	Tumour Micro Environment
CAFs	Cancer-Associated Fibroblasts
ECM	Extra Cellular Matrix
EMT	Epithelial/Endothelial-Mesenchymal Transition
ATR	Attenuated Total Reflectance
IR	InfraRed
NIR	Near InfraRed
NMR	Nuclear Magnetic Resonance
MFI	Microscope Fluorescence Intensity
ROI	Region of Interest
DMEM	Dulbecco's Modified Eagle's Medium
PBS	Phosphate-Buffered Saline
MTT	4,5-(dimethylthiazol-2-yl)-2,5-diphenyltetrazolium bromide
DMSO	Dimethyl Sulfoxide
DABCO	1,4-diazabicyclo[2.2.2]octane
THF	Tetrahydrofuran
rt	room temperature
FBS	Fetal Bovine Serum
UV–Vis	Ultra Violet Visible
MCF-7	Michigan Cancer Foundation-7
HDF	Human Dermal Fibroblast
HEK-293	Human Embryonic Kidney
U-87 MG	Uppsala 87 Malignant Glioma
HepG2	Hepatoblastoma
IC_{50}	Inhibitory Concentration
ANOVA	Analysis of Variance
SD	Standard Deviation
LSM	Laser Scanning Microscope

Supplementary Information

The online version contains supplementary material available at https://doi.org/10.1186/s12880-024-01488-x.

Supplementary Material 1
Supplementary Material 2
Supplementary Material 3
Supplementary Material 4
Supplementary Material 5
Supplementary Material 6
Supplementary Material 7
Supplementary Material 8
Supplementary Material 9
Supplementary Material 10
Supplementary Material 11
Supplementary Material 12
Supplementary Material 13
Supplementary Material 14
Supplementary Material 15
Supplementary Material 16
Supplementary Material 17
Supplementary Material 18
Supplementary Material 19
Supplementary Material 20
Supplementary Material 21
Supplementary Material 22
Supplementary Material 23
Supplementary Material 24
Supplementary Material 25
Supplementary Material 26
Supplementary Material 27
Supplementary Material 28
Supplementary Material 29
Supplementary Material 30
Supplementary Material 31
Supplementary Material 32
Supplementary Material 33
Supplementary Material 34
Supplementary Material 35
Supplementary Material 36
Supplementary Material 37
Supplementary Material 38
Supplementary Material 39
Supplementary Material 40
Supplementary Material 41
Supplementary Material 42
Supplementary Material 43
Supplementary Material 44
Supplementary Material 45
Supplementary Material 46

Acknowledgements
Not applicable.

Author contributions
AC performed and analysed data regarding cell toxicity and cellular uptake studies. LV performed the synthesis and characterization of the compound. PS performed the optical characterisation of the compound. AP and GC supervised the work. All authors read and approved the final manuscript.

Funding
No external funding was received for this research.

Data availability
The datasets used and/or analysed during the current study are available from the corresponding author on reasonable request.

Declarations

Ethics approval and consent to participate
Not applicable.

Consent for publication
Not applicable.

Competing interests
The authors declare no competing interests.

Received: 26 June 2024 / Accepted: 4 November 2024
Published online: 20 November 2024

References

1. Nair M, Sandhu SS, Sharma AK. Cancer molecular markers: a guide to cancer detection and management. Semin Cancer Biol. 2018;52:39–55. https://doi.org/10.1016/j.semcancer.2018.02.002.
2. NHS England. Screening and earlier diagnosis 2024. www.england.nhs.uk/cancer/early-diagnosis/screening-and-earlier-diagnosis/
3. Cheng Q, Lau WM, Chew SH, Ho TH, Tay SK, Hui KM. Identification of molecular markers for the early detection of human squamous cell carcinoma of the uterine cervix. Br J Cancer. 2002;86:274–81. https://doi.org/10.1038/sj/bjc/6600038.
4. Rader JS, Gerhard DS, O'Sullivan MJ, Li Y, Li L, Liapis H, et al. Cervical intraepithelial neoplasia III shows frequent allelic loss in 3p and 6p. Genes Chromosomes Cancer. 1998;22:57–65. https://doi.org/10.1002/(SICI)1098-2264(199805)22:1<57::AID-GCC8>3.0.CO;2-6.
5. Ye F, Dewanjee S, Li Y, Jha NK, Chen ZS, Kumar A, et al. Advancements in clinical aspects of targeted therapy and immunotherapy in breast cancer. Mol Cancer. 2023;22:105. https://doi.org/10.1186/s12943-023-01805-y.
6. Zhang Y, Schnabel CA, Schroeder BE, Jerevall PL, Jankowitz RC, Fornander T, et al. Breast cancer index identifies early-stage estrogen receptor-positive breast cancer patients at risk for early- and late-distant recurrence. Clin Cancer Res. 2013;19:4196–205. https://doi.org/10.1158/1078-0432.CCR-13-0804.
7. Filho OM, Ignatiadis M, Sotiriou C. Genomic Grade Index: an important tool for assessing breast cancer tumor grade and prognosis. Crit Rev Oncol Hematol. 2011;77:20–9. https://doi.org/10.1016/j.critrevonc.2010.01.011.
8. Young KC, Oduko JM. Radiation doses received in the United Kingdom breast screening programme in 2010 to 2012. Br J Radiol. 2016;89:20150831. https://doi.org/10.1259/bjr.20150831.
9. Olchowy C, Cebulski K, Łasecki M, Chaber R, Olchowy A, Kałwak K, et al. The presence of the gadolinium-based contrast agent depositions in the brain and symptoms of gadolinium neurotoxicity-A systematic review. PLoS ONE. 2017;12:e0171704. https://doi.org/10.1371/journal.pone.0171704.
10. Su Y, Liu S, Guan Y, Xie Z, Zheng M, Jing X. Renal clearable hafnium-doped carbon dots for CT/Fluorescence imaging of orthotopic liver cancer. Biomaterials. 2020;255:120110. https://doi.org/10.1016/j.biomaterials.2020.120110.
11. Dasari S, Wudayagiri R, Valluru L. Cervical cancer: biomarkers for diagnosis and treatment. Clin Chim Acta. 2015;445:7–11. https://doi.org/10.1016/j.cca.2015.03.005.
12. Villegas-Pineda JC, Ramírez-de-Arellano A, Bueno-Urquiza LJ, Lizarazo-Taborda M, del Pereira-Suárez R. Cancer-associated fibroblasts in gynecological malignancies: are they really allies of the enemy? Front Oncol. 2023;13:1106757. https://doi.org/10.3389/fonc.2023.1106757.
13. Li Y, Wang C, Huang T, Yu X, Tian B. The role of cancer-associated fibroblasts in breast cancer metastasis. Front Oncol. 2023;13:1194835. https://doi.org/10.3389/fonc.2023.1194835.
14. Wallace TC, Blusztajn JK, Caudill MA, Klatt KC, Natker E, Zeisel SH, et al. The underconsumed and underappreciated essential nutrient. Nutr Today. 2018;53:240–53. https://doi.org/10.1097/NT.0000000000000302.
15. Morozov VI, Kalinski MI, Sakuta GA, Choline. The role in Cell Life and potential Biomarker Molecule. Hum Biology Rev. 2013;2:77–89.
16. Ackerstaff E, Glunde K, Bhujwalla ZM. Choline Phospholipid metabolism: a target in Cancer cells? J Cell Biochem. 2003;90:525–33. https://doi.org/10.1002/jcb.10659.
17. Glunde K, Ackerstaff E, Mori N, Jacobs MA, Bhujwalla ZM. Choline Phospholipid Metabolism in Cancer: consequences for Molecular Pharmaceutical interventions 2006;3.5:496–506. https://doi.org/10.1021/mp060067e
18. Glunde K, Jacobs MA, Bhujwalla ZM. Choline metabolism in cancer: implications for diagnosis and therapy. Http://DxDoiOrg/101586/1473715966821. 2014;6:821–9. https://doi.org/10.1586/14737159.6.6.821.
19. RADIOACTIVE TRACERS - Advantages. and disadvantages table in A Level and IB Applied Science n.d. https://getrevising.co.uk/grids/radioactive-tracers
20. Villa AM, Caporizzo E, Papagni A, Miozzo L, Del Buttero P, Grilli MD, et al. Choline and phosphatidylcholine fluorescent derivatives localization in carcinoma cells studied by laser scanning confocal fluorescence microscopy. Eur J Cancer. 2005;41:1453–9. https://doi.org/10.1016/J.EJCA.2005.02.028.
21. Minotti G, Menna P, Salvatorelli E, Cairo G, Gianni L, Anthracyclines. Molecular advances and pharmacologic developments in Antitumor Activity and Cardiotoxicity. Pharmacol Rev. 2004;56:185–229. https://doi.org/10.1124/PR.56.2.6.
22. Peng HY, Zhang G, Sun R, Xu YJ, Ge JF. Fluorescent probes based on acridine derivatives and their application in dynamic monitoring of cell polarity variation. Analyst. 2022;147:5231–8. https://doi.org/10.1039/d2an01449a.
23. Nunhart P, Konkoľová E, Janovec L, Jendželovský R, Vargová J, Ševc J, et al. Fluorinated 3,6,9-trisubstituted acridine derivatives as DNA interacting agents and topoisomerase inhibitors with A549 antiproliferative activity. Bioorg Chem. 2020;94:103393. https://doi.org/10.1016/j.bioorg.2019.103393.
24. Hevey R. The role of Fluorine in Glycomimetic Drug Design. Chem – Eur J. 2021;27:2240–53. https://doi.org/10.1002/CHEM.202003135.
25. Vaghi L, Rizzo F, Pedrini J, Mauri A, Meinardi F, Cosentino U, et al. Bypassing the statistical limit of singlet generation in sensitized upconversion using fluorinated conjugated systems. Photochemical Photobiological Sci. 2022;21:913–21. https://doi.org/10.1007/s43630-022-00225-z.
26. Mosmann T. Rapid colorimetric assay for cellular growth and survival: application to proliferation and cytotoxicity assays. J Immunol Methods. 1983;65:55–63. https://doi.org/10.1016/0022-1759(83)90303-4.
27. Satheeshkumar R, Edatt L, Muthusankar A, Sameer Kumar VB, Rajendra Prasad KJ. Synthesis of Novel Quin[1,2-b]acridines: in Vitro cytotoxicity and molecular Docking studies. Polycycl Aromat Compd. 2021;41:1631–45. https://doi.org/10.1080/10406638.2019.1689515.
28. Shihan MH, Novo SG, Le Marchand SJ, Wang Y, Duncan MK. A simple method for quantitating confocal fluorescent images. Biochem Biophys Rep. 2021;25:100916. https://doi.org/10.1016/j.bbrep.2021.100916.
29. Mei Q, Shi Y, Hua Q, Tong B. Phosphorescent chemosensor for hg 2 + based on an iridium (iii) complex coordinated with 4-phenylquinazoline and carbazole dithiocarbamate. RSC Adv. 2015;5:74924–31. https://doi.org/10.1039/C5RA09609J.
30. Papagni A, del Buttero P, Moret M, Sassella A, Miozzo L, Ridolfi G. Synthesis and Properties of some derivatives of 1,2,3, 4-Tetrafluoroacridine for Solid State Emitting systems. Chem Mater. 2003;15:5010–8. https://doi.org/10.1021/cm034504i.
31. Liu K, Brivio M, Xiao T, Norwood VM, Kim YS, Jin S, et al. Modular synthetic routes to fluorine-containing halogenated phenazine and Acridine agents that Induce Rapid Iron Starvation in Methicillin-Resistant Staphylococcus aureus Biofilms. ACS Infect Dis. 2022;8:280–95. https://doi.org/10.1021/acsinfecdis.1c00402.
32. Kienzler MA, Reiner A, Trautman E, Yoo S, Trauner D, Isacoff EY. A red-shifted, fast-relaxing azobenzene photoswitch for visible light control of an ionotropic glutamate receptor. J Am Chem Soc. 2013;135:17683–6. https://doi.org/10.1021/ja408104w.
33. Zhang B, Dou Z, Xiong Z, Wang N, He S, Yan X, et al. Design, synthesis and biological research of novel N-phenylbenzamide-4-methylamine acridine derivatives as potential topoisomerase I/II and apoptosis-inducing agents. Bioorg Med Chem Lett. 2019;29:126714. https://doi.org/10.1016/j.bmcl.2019.126714.
34. Kozurkova M. Acridine derivatives as inhibitors/poisons of topoisomerase II. J Appl Toxicol. 2022;42:544–52. https://doi.org/10.1002/jat.4238.
35. Fahim AM, Tolan HEM, El-Sayed WA. Synthesis of novel 1,2,3-triazole based acridine and benzothiazole scaffold N-glycosides with anti-proliferative activity, docking studies, and comparative computational studies. J Mol Struct. 2022;1251:131941. https://doi.org/10.1016/j.molstruc.2021.131941.
36. Haider MR, Ahmad K, Siddiqui N, Ali Z, Akhtar MJ, Fuloria N, et al. Novel 9-(2-(1-arylethylidene)hydrazinyl)acridine derivatives: Target Topoisomerase 1 and growth inhibition of HeLa cancer cells. Bioorg Chem. 2019;88:102962. https://doi.org/10.1016/j.bioorg.2019.102962.
37. Adriá-Cebrián J, Guaita-Esteruelas S, Lam EWF, Rodríguez-Balada M, Capellades J, Girona J, et al. Mcf-7 drug resistant cell lines switch their lipid metabolism to triple negative breast cancer signature. Cancers (Basel). 2021;13:5871. https://doi.org/10.3390/cancers13235871.
38. Al-Saeedi F, Smith T, Welch A. [Methyl-3H]-choline incorporation into MCF-7 cells: correlation with proliferation, choline kinase and Phospholipase D Assay. Anticancer Res. 2007;27:901–6.

39. Bolan PJ. Magnetic resonance spectroscopy of the breast: current status. Magn Reson Imaging Clin N Am. 2013;21:625–39. https://doi.org/10.1016/j.mric.2013.04.008.
40. Roppongi M. Mitsuru Izumisawa ·, Terasaki · Kazunori, Muraki · Yasushi, Shozushima · Masanori. 18F-FDG and 11 C-choline uptake in proliferating tumor cells is. Depend cell Cycle vitro. 2019;33:237–43. https://doi.org/10.1007/s12149-018-01325-6.
41. Iorio E, Mezzanzanica D, Alberti P, Spadaro F, Ramoni C, D'Ascenzo S, et al. Alterations of Choline Phospholipid metabolism in ovarian tumor progression. Cancer Res. 2005;65:9369–76. https://doi.org/10.1158/0008-5472.CAN-05-1146.
42. Guy GR. Murray2 AW. Tumor promoter stimulation of phosphatidylcholine turnover in HeLa cells. Cancer Res. 1980;42:1980–5.
43. Quail DF, Joyce JA. Microenvironmental regulation of tumor progression and metastasis. Nat Med. 2013;19:1423–37. https://doi.org/10.1038/nm.3394.
44. Wessels DJ, Pradhan N, Park YN, Klepitsch MA, Lusche DF, Daniels KJ, et al. Reciprocal signaling and direct physical interactions between fibroblasts and breast cancer cells in a 3D environment. PLoS ONE. 2019;14:e0218854. https://doi.org/10.1371/journal.pone.0218854.
45. Yang D, Liu J, Qian H, Zhuang Q. Cancer-associated fibroblasts: from basic science to anticancer therapy. Exp Mol Med. 2023;55:1322–32. https://doi.org/10.1038/s12276-023-01013-0.
46. Liu X, Shan K, Shao X, Shi X, He Y, Liu Z, et al. Nanotoxic effects of silver nanoparticles on normal HEK-293 cells in comparison to cancerous hela cell line. Int J Nanomed. 2021;16:753–61. https://doi.org/10.2147/IJN.S289008.
47. Katz-Brull R, Seger D, Rivenson-Segal D, Rushkin E, Degani H. Metabolic markers of breast Cancer: enhanced choline metabolism and reduced choline-ether-phospholipid synthesis. Cancer Res. 2002;62:1966–70.
48. Aboagye EO, Bhujwalla ZM. Malignant Transformation alters membrane Choline Phospholipid metabolism of human mammary epithelial cells. Cancer Res. 1999;59:80–4.

Publisher's note